Geophysical Research Letters

RESEARCH LETTER
10.1029/2023GL104642

Key Points:

- Evaporation causes groundwater and solutes to upwell from deep sediments to the surface, resulting in near-surface solute accumulation
- Heterogeneity causes strain-dominated and vorticity-dominated flow regions to coexist at small spatial scales along preferential flow paths
- Upwelling groundwater creates distinct mixing hotspots that differ spatially from those generated by large-scale hydraulic gradients

Supporting Information:

Supporting Information may be found in the online version of this article.

Correspondence to:

X. Geng,
gengxiaolong@gmail.com

Citation:

Geng, X., Boufadel, M. C., Li, H., Na Nagara, V., & Lee, K. (2023). Impacts of evaporation-induced groundwater upwelling on mixing dynamics in shallow wetlands. *Geophysical Research Letters*, *50*, e2023GL104642. https://doi.org/10.1029/2023GL104642

Received 22 MAY 2023
Accepted 25 JUL 2023
Corrected 21 AUG 2023

This article was corrected on 21 AUG 2023. See the end of the full text for details.

Author Contributions:

Conceptualization: Xiaolong Geng, Michel C. Boufadel
Funding acquisition: Xiaolong Geng, Michel C. Boufadel, Kenneth Lee
Investigation: Xiaolong Geng, Hailong Li, Viravid Na Nagara
Methodology: Xiaolong Geng, Michel C. Boufadel
Project Administration: Hailong Li

Impacts of Evaporation-Induced Groundwater Upwelling on Mixing Dynamics in Shallow Wetlands

Xiaolong Geng[1,2], Michel C. Boufadel[3], Hailong Li[4], Viravid Na Nagara[3], and Kenneth Lee[5]

[1]Department of Earth Sciences, University of Hawai'i at Mānoa, Honolulu, HI, USA, [2]Water Resources Research Center, University of Hawai'i at Mānoa, Honolulu, HI, USA, [3]Department of Civil and Environmental Engineering, New Jersey Institute of Technology, Newark, NJ, USA, [4]State Environmental Protection Key Laboratory of Integrated Surface Water-Groundwater Pollution Control, School of Environmental Science & Engineering, Southern University of Science and Technology, Shenzhen, China, [5]Department of Fisheries and Oceans, Dartmouth, NS, Canada

Abstract Groundwater mixing dynamics play a crucial role in the biogeochemical cycling of shallow wetlands. In this paper, we conducted groundwater simulations to investigate the combined effects of evaporation and local heterogeneity on mixing dynamics in shallow wetland sediments. The results show that evaporation causes groundwater and solutes to upwell from deep sediments to the surface. As the solute reaches the surface, evaporation enhances the accumulation of the solute near the surface, resulting in a higher solute concentration than in deep sediments. Mapping of flow topology reveals that local heterogeneity generates spatially varied mixing patterns mainly along preferential flow pathways. The upwelling of groundwater induced by surface evaporation through heterogeneous sediments is likely to create distinct mixing hotspots that differ spatially from those generated by lateral preferential flows driven by large-scale hydraulic gradients, which enhances the overall mixing in the subsurface. These findings have strong implications for biogeochemical processing in wetlands.

Plain Language Summary In shallow wetlands, groundwater mixing and exchange have been identified as critical factors affecting biogeochemical cycling and transformation in sediments. Our results for the first time demonstrate evaporation causes a significant upwelling of groundwater and solutes from deep sediments to the surface. As the solute reaches the surface, evaporation enhances the accumulation of the solute near the surface, resulting in a higher solute concentration than in deep sediments. Mapping of flow topology, including the Okubo-Weiss parameter and dilution index, reveals that evaporation and local heterogeneity generates dynamic mixing patterns along preferential flow pathways. Such mixing mechanisms would strongly affect biogeochemical conditions in near-surface sediments of shallow wetlands, which have strong implications for wetland ecosystems.

1. Introduction

Among the most productive ecosystems on the earth, wetlands play an integral role in regulating the ecology of watersheds, including hydrologic transfers and storage of water, biogeochemical transformations, and primary productivity and decomposition (Bhowmik, 2022; Richardson, 1994). Wetlands also provide habitats and food webs for an immense variety of species, such as microbes, plants, insects, amphibians, reptiles, birds, fish, and mammals (Douglas et al., 2005). Wetland groundwater flow involves complex interactions with various surface hydrological processes, providing primary controls on biogeochemical cycling and transformation of such elements as carbon, nutrients (e.g., N, P, and S), metals (e.g., Fe and Mn), microbial community structure in sediments (Sadat-Noori & Glamore, 2019; F. Wang et al., 2022; Wilson et al., 2015). It also affects terrestrial chemical fluxes entering surface waters via terrestrial groundwater discharge, which has strong implications for ecological zonation and productivity in wetlands (Wang & Cai, 2004; Wilson & Gardner, 2006).

There are multiple driving factors that control groundwater flow and associated solute transport in wetland systems (Guimond & Tamborski, 2021; Xin et al., 2022; Zhao et al., 2016). Wetlands are classified into tidal wetlands and non-tidal wetlands. Tidal wetlands are found along coastlines, and can contain only freshwater, but are influenced by tides. Tidal action facilitates the exchange of water and chemicals between tidal creeks and wetlands, which in turn supports the overall hydrological and biogeochemical functioning of wetland ecosystems (Armstrong et al., 1985; Balke et al., 2016; Xiao et al., 2019). Non-tidal wetlands are more found around inland

Supervision: Michel C. Boufadel, Hailong Li, Viravid Na Nagara, Kenneth Lee
Validation: Xiaolong Geng, Michel C. Boufadel
Writing – original draft: Xiaolong Geng
Writing – review & editing: Michel C. Boufadel, Hailong Li, Viravid Na Nagara, Kenneth Lee

areas, not subject to tidal influence. They are typically areas where the groundwater table is shallow at or near the surface (Doss, 1993). Instead of tides, groundwater flow in non-tidal wetlands is controlled by the hydraulic connection with surrounding watersheds. Terrestrial freshwater recharge creates large-scale hydraulic gradients that drive groundwater flow from uplands to wetland depressions (de la Fuente and Meruane, 2017; Thibodeau et al., 1998). Such lateral groundwater flows could transport inland-derived nutrients into wetland areas and therefore affect the transformation and storage of nutrients in wetland soil. Terrestrial freshwater recharge into wetlands is influenced by a multitude of hydrological and environmental factors. For instance, high precipitation rates and significant differences in elevation between uplands and low-lying wetland platforms could create steep lateral hydraulic gradients (de la Fuente and Meruane, 2017). This in turn enhances the transport of terrestrial freshwater and associated solutes into the wetlands (Davy et al., 2011; Zedler et al., 1999). Spatial heterogeneity of sediment permeability could also impact the subsurface flow and transport pathways in wetlands. Wetland sediments are often heterogeneous with macropores, rip-up clasts, and amalgamations of terrestrial organic matters such as leaves, sticks, and fine-grained organic matter (Guimond et al., 2020; Harvey & Nuttle, 1995; Moffett et al., 2012; Sawyer, 2015). Numerous studies have identified that local heterogeneity can exert a strong control on flow and nutrient transport in aquatic sediments (Harvey et al., 1995; Sawyer, 2015; Xu et al., 2021).

As a fundamental component of the hydrologic cycle, evaporation is an important driver for subsurface flow and transport processes in wetlands (Li et al., 2005; Silvestri et al., 2005; Zhang et al., 2014). Previous studies identified the upwelling of groundwater due to the evaporation from the sediment surface (Geng & Boufadel, 2015; Geng et al., 2016a). In wetland systems with a shallow groundwater table, the near-surface region usually has a relatively high water content (due to strong capillary forces), which facilitates pore water evaporation from the sediments (Mahfouf & Noilhan, 1991; Xin et al., 2017). The shallow groundwater table also builds a strong hydraulic connection between the evaporation front and deep surrounding groundwater, which efficiently replenishes the loss of water evaporated near the wetland surface, resulting in a sustainable evaporation rate on the surface (Liu et al., 2022). In wetlands, the large-scale hydraulic gradients induce lateral groundwater flow to the depression areas, while strong evaporation drives pore water to flow upward. Therefore, lateral hydraulic gradients interacting with evaporation as well as local heterogeneity might induce very complex driving mechanisms that transport groundwater flow and solutes/contaminants from deep sediments toward the wetland surface (Figure 1). Such driving mechanisms are expected to be more obvious in the depression regions of non-tidal wetlands, due to the shallow groundwater table and relatively long exposure time to the air compared to the regions periodically inundated by tides. However, the impacts of evaporation and associated groundwater upwelling on wetland subsurface transport behaviors have not been investigated, especially taking into account geologic heterogeneity. These water and solute mixing dynamics are critical for understanding aspects of wetland systems such as subsurface biogeochemical transformation, contaminant fate, and ecosystem function.

In this work, we use numerical simulations to illustrate the effects of evaporation-induced groundwater upwelling on the mixing dynamics of subsurface flow and solute in shallow wetlands. Simulations of subsurface flow and solute transport were conducted through a 2-D density-dependent, variably saturated model, considering evaporation impacts on the surface for both homogeneous and heterogeneous sediments. Tempo-spatial evolution of subsurface pore-water flow and solute transport in response to interplay of lateral hydraulic gradient and surface evaporation was quantified.

2. Methodology

2.1. Representation of Heterogeneous K Field

Geophysical fields (e.g., hydraulic conductivity K fields) have been widely observed to be self-similar or so-called scaling invariant (Boufadel et al., 2000; Peitgen & Saupe, 1988; Schertzer & Lovejoy, 2011). Scaling properties of a K field at the support scale h can be characterized using the sth order structure function:

$$\langle |\Delta K_h|^s \rangle \sim h^{-\xi(s)}, \tag{1}$$

where the function $\xi(s)$ is the structure function exponent. In this study, heterogeneous K fields were assumed to follow multifractal scaling, which captures both Gaussian and non-Gaussian statistics. Heterogeneous K fields were generated using the universal multifractal (UM) model (Geng, Boufadel, Lee, & An, 2020; Tessier et al., 1993) by adopting the multifractal properties analyzed from the in-situ permeability data

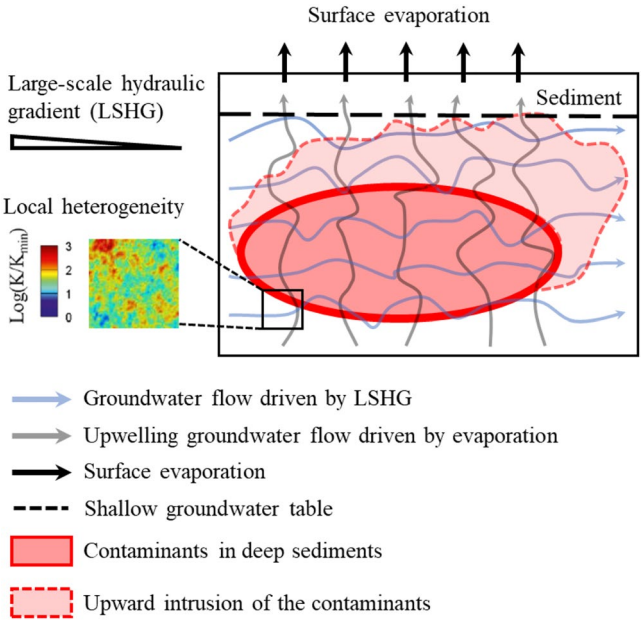

Figure 1. Schematics of groundwater flow and contaminant transport in heterogeneous aquatic sediments, where large-scale hydraulic gradients and surface evaporation alternate as the primary driving force. The blue arrow lines illustrate the flow paths generated by the hydraulic gradient, while the gray arrow lines denote the upwelling groundwater flow caused by surface evaporation. The red shades represent the upward intrusion of contaminants in deep sediments, driven by the upwelling groundwater flow.

measured in Castle et al. (2004) as input, which represents a wide range of fluvial to marine depositional settings, including wave-dominated and tide-dominated nearshore-marine environments. In the UM model, the function $\xi(s)$ is expressed as follows (Pecknold et al., 1993; Schertzer & Lovejoy, 1987):

$$\xi = sH - \frac{c1}{\alpha - 1}(s^{\alpha} - s), \tag{2}$$

Where α ($0 < \alpha \leq 2$) is the multifractal parameter, measuring departure from monofractal behavior defined by $\alpha = 0$; $c1$ is the codimension parameter, measuring the degree of intermittency; and H is the Hurst exponent linked to the degree of scale invariant smoothing. To mitigate any potential bias originating from the boundaries, the 2D fractal K field was generated over 512×512 cells at 0.05×0.05 m resolution, and the central 61×201 was extracted and used for groundwater flow and transport modeling. The geometric mean of K was maintained at 1.0×10^{-4} m/s. The generated multifractal fields were tested to preserve the same underlying statistics as the measurement fields by comparing observed and simulated structure function exponents (i.e., ξ). The details of generating multifractal K fields are described in Geng, Boufadel, Rajaram et al. (2020). A homogeneous case with the equivalent K to the heterogeneous case was also simulated for comparison.

2.2. Groundwater Flow and Solute Transport Model

Subsurface flow and solute transport were simulated using the variably saturated density-dependent model MARUN (Boufadel et al., 1999; Geng & Boufadel, 2015, 2017; Geng, Pan, et al., 2016; Li et al., 2008). The simulated domain is 10 m wide and 3 m deep to represent near-surface wetland sediments (Figure S1 in Supporting Information S1). The grid resolution of the simulated domain is 0.05 m in both directions. The mesh was made fine enough to meet the strict criterion for the grid Peclet number to be less than or equal to 2.0 (Zheng & Bennett, 2002). The time step selected for the MARUN simulation was 6.0 s, ensuring that the grid Courant number remained below 0.5. In the model, the convergence criterion for the Picard iteration of the pressure head was set at 10^{-5} m. At the inflow boundary, a shallow groundwater table was assumed, which was set 15 cm below the surface. A mild hydraulic gradient of 2×10^{-3} was adopted in the model, resulting in a 2 cm drop in the groundwater table at the outflow boundary. To investigate the impacts of evaporation-induced groundwater upwelling on the movement of solute from deep sediments toward the surface, we assumed the presence of ions in solution at the concentration of 0.6 mg/L at a depth of 50 cm below the surface.

2.3. Evaporation

Evaporation was applied at the surface every 12 hr to represent the daily fluctuations of evaporation effects. We established the meteorological parameters of 40% relative humidity, 27°C temperature, and 2.5 m/s wind speed to simulate a typical summer climate with relatively dry conditions (Figure S2 in Supporting Information S1). An evaporation flux, E_g, was calculated using the bulk aerodynamic approach (Mahfouf & Noilhan, 1991):

$$E_g = \frac{\rho_{\text{air}}}{\rho_{\text{water}} R_{\text{air}}}(q_g - q_{\text{air}}). \tag{3}$$

Where ρ_{air} and ρ_{water} denote the density of air and freshwater, respectively, q_a and q_g denote the air and surface relative humidity, respectively, and R_{air} is the aerodynamic resistance, expressed as $94.909 \times u^{-0.9036}$, where u represents the wind speed (m/s) at the atmospheric reference level (~2 m above the soil surface). There are numerous models that have been developed to estimate the aerodynamic resistance (Ghiat et al., 2021). In this paper, we chose to adopt the empirical relationship between aerodynamic resistance and wind speed as proposed by Liu et al. (2006), which has proven its validity across both bare soil surface and maize fields. Cauchy boundary

condition was adopted in the MARUN model to simulate solute accumulation below the soil surface due to evaporation, expressed as follows (Geng & Boufadel, 2015):

$$\left(\vec{q}c - \beta\phi S D \cdot \nabla c\right) \cdot \vec{n} = 0, \tag{4}$$

where $\vec{q}$ is the Darcy flux vector, c is the solute concentration, β is the density ratio between actual water density to freshwater density, ϕ is the porosity of the porous medium, S is the soil moisture, D represents the physical dispersion tensor, $\vec{n}$ is the vector normal to the boundary.

2.4. Metrics of Groundwater Flow and Solute Transport

In this work, flow topology was used to characterize the mixing strength in heterogeneous porous media (de Barros et al., 2012; Sposito, 2001). In particular, de Barros et al. (2012) revealed that flow topology categorizes a flow field as strain-dominated and vorticity-dominated regions. Within strain-dominated regions, a solute plume will be stretched and deformed, which increases the interface between the plume and surrounding clean water, and therefore enhances the mixing of solute in pore spaces. By contrast, within vorticity-dominated regions, the solute plume will only be spun by local fluid rotation, which results in less local mixing of the solute with the surrounding groundwater. A measure of flow topology is the Okubo-Weiss parameter, Θ, which depends on shear and stretching deformation and vorticity:

$$\Theta = \left(\frac{\partial q_x}{\partial x} - \frac{\partial q_z}{\partial z}\right)^2 + \left(\frac{\partial q_z}{\partial x} + \frac{\partial q_x}{\partial z}\right)^2 - \left(\frac{\partial q_z}{\partial x} - \frac{\partial q_x}{\partial z}\right)^2 \tag{5}$$

where q_x and q_z denote the Darcy fluxes in the horizontal and vertical directions, respectively. The three terms on the right-hand side represent the normal and shear components of strain (s_n and s_s) and the relative vorticity of the flow, respectively. The value of Θ allows the classification of flow fields into three types based on the value of the standard deviation of the field, σ_{ow} (Isern-Fontanet et al., 2004). These are: a vorticity-dominated region ($\Theta < -0.2\sigma_{ow}$), a strain-dominated region ($\Theta > 0.2\sigma_{ow}$), and a background sheared flow field ($|\Theta| \leq 0.2\sigma_{ow}$).

A local-scale analysis of mixing strength relies on the measure of dilution, defined as the dilution index, E, which has also been introduced herein to characterize the mixing patterns of solutes in heterogeneous aquatic sediments (de Barros et al., 2012; Kitanidis, 1994), and we used it in our prior work (Geng, Boufadel, Lee, & An, 2020; Geng, Heiss, et al., 2020; Geng, Michael et al., 2020). To investigate impacts of evaporation on the mixing strength, we integrated $E(x, z, t)$ over 12-hr periods when evaporation was on and off, respectively:

$$E(x, z) = \int_0^T \frac{dE(x, z, t)}{dt} dt, \tag{6}$$

where the integration is calculated at each element over a particular time to represent overall local-scaling mixing at that location. The dilution index at each node and specific time is calculated using the simulation results obtained from the MARUN model.

Forward particle-tracking was conducted to reveal the upwelling flow pathways and associated transit times within the simulated domain. A particle tracking code, NEMO3D (Geng, Boufadel, Rajaram, et al., 2020; Geng et al., 2014, 2016b), was used for these simulations. The neutrally buoyant particles were released 50 cm below the surface at a 10 cm horizontal interval at the initial time, and the simulated transient velocity field was used for displacing the particle locations at each time step without allowing for dispersion.

3. Results

Figure 2 shows that without evaporation, lateral groundwater flow pathways were simulated for both heterogeneous and homogeneous cases, which are mainly driven by the large-scale hydraulic gradient. By contrast, as evaporation occurred on the sediment surface, the direction of groundwater flow was altered, causing it to flow upwards toward the surface (Figures 2b and 2c). In particular, the upwelling groundwater flow paths were observed at depth of 1 m below the surface. This indicates that evaporation affected groundwater flow from deep sediment pores to the surface. Our simulation results also show that local heterogeneity caused the perturbation

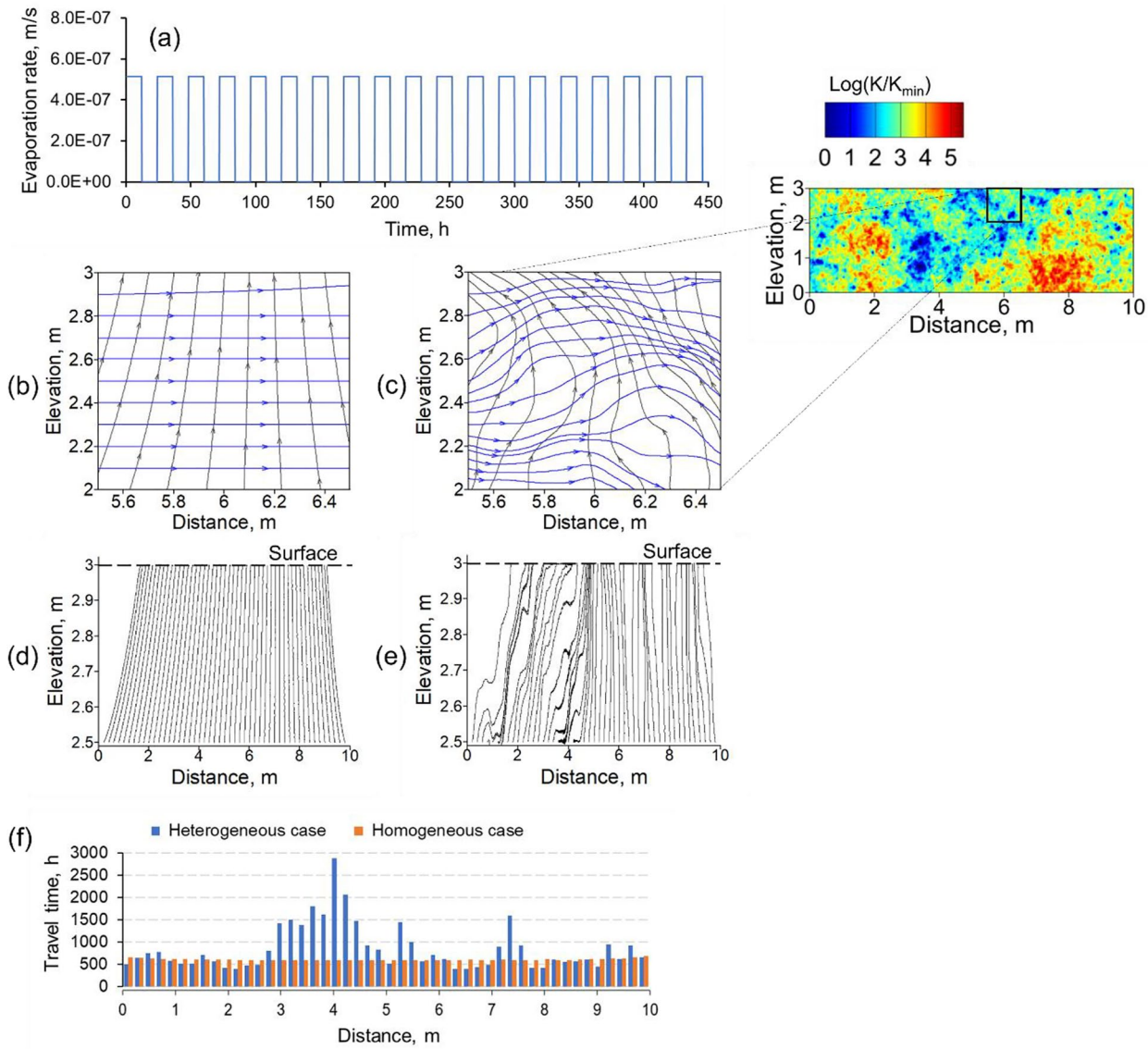

Figure 2. (a) Simulated evaporation rate on the sediment surface, (b, c) groundwater flow paths driven by the large-scale hydraulic gradient (blue arrow lines) and surface evaporation (black arrow lines), respectively, for homogeneous and heterogeneous cases, (d, e) upwelling trajectory of particles released at the deep location 0.5 m below the ground surface for homogeneous and heterogeneous cases, respectively, and (f) travel time required for the released particles to reach the sediment surface, for both homogeneous and heterogeneous cases. The heterogeneous hydraulic conductivity (K) field generated using the Universal Multifractal (UM) model is shown in (c).

of the groundwater flow pathways in both lateral and vertical directions (Figure 2c). For the heterogeneous case, a centimeter-scale upwelling of the lateral flow paths (i.e., without evaporation) is observed at the distance between 6 and 6.5 m. This is most likely due to the existence of preferential groundwater paths flowing through high permeability zones adjacent to low permeability zone. This highlights the important impact of local heterogeneity on groundwater flow paths.

The particle tracking results demonstrate the upward movements of particles released from deep sediments to the surface due to evaporation for both homogeneous and heterogeneous cases (Figures 2d and 2e). The particles released in the homogeneous sediments demonstrated consistent upwelling trajectories from deep sediments to the surface. By contrast, a significant perturbation of the particle trajectories was observed for the heterogeneous case. Due to local heterogeneity, some particle trajectories converged and formed preferential pathways from deep sediments to the surface. It resulted in a nonuniform spatial distribution of travel time required for the particles released from deep sediments to reach the surface (Figure 2f). The mean ± standard deviation of the travel

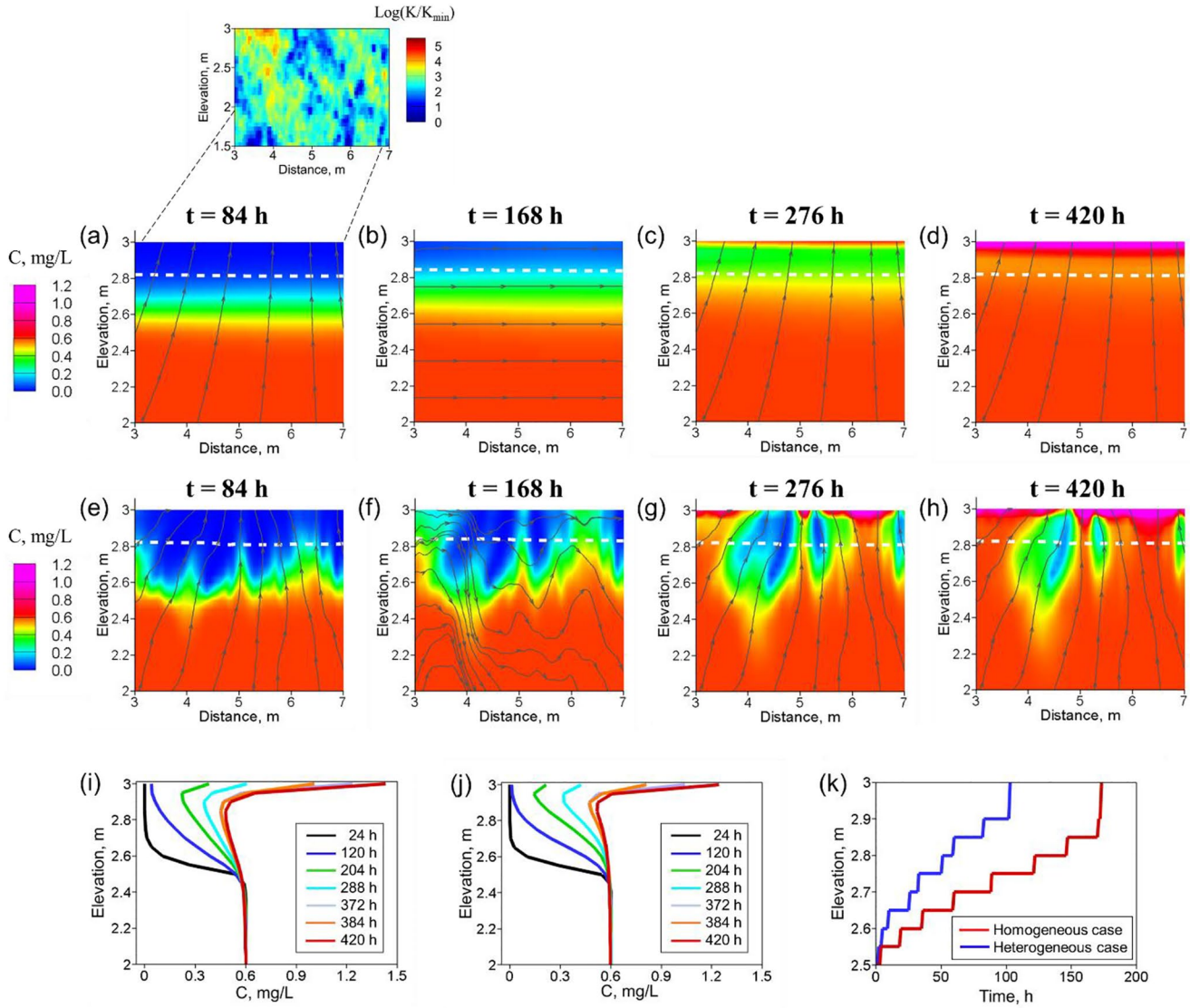

Figure 3. Concentration contours depicting the upward intrusion of the solute in deep sediment due to evaporation-induced upwelling groundwater flow for (a–d) homogeneous case and (e–h) heterogeneous case. (i, j) The horizontal-average concentration distribution below the surface at different times for homogeneous and heterogeneous cases, respectively. (k) The upward intrusion of the solute plume as a function of time, with the delineation of the plumes' edge where the concentration was 20% of the maximum (i.e., 0.12 mg/L).

time for the homogeneous case was 602 hr ± 22 hr, while it varied significantly for the heterogeneous case, ranging from 386 to 2890 hr with a mean and standard deviation of 847 hr ± 532 hr. The extremely long travel time at certain locations (e.g., the distance between 3 and 5 m) is because fairly low hydraulic conductivity limited the travel speed of the particles released within the low permeability zones, and therefore dramatically increased the travel time of the particles before they reached the upwelling preferential flow pathways.

Evaporation-induced upwelling groundwater flow induces the intrusion of solute from deep sediments to the surface. For the homogeneous case, alternating evaporation effects on the sediment surface drove the solute to migrate upward from deep sediments toward the surface (Figures 3a and 3b). As the solute reached the surface, subsequent evaporation accumulated the solute near the surface and significantly elevated the solute concentration near the sediment surface. According to the simulations, due to evaporation, the concentration near the surface increased to twice the initial concentration of solute set in deep sediments (Figure 3c). As a result, the concentration gradient reversed, with a higher concentration near the sediment surface. This caused the near-surface solute plume to disperse downwards, leading to elevated solute concentration at deeper locations (Figure 3d).

The upward intrusion of the solute from deep sediments was also observed for the heterogeneous case but with large spatial variability (Figure 3e). It shows that preferential flow accelerated the evaporation-induced upward movement of the solute through high permeability zones. Interestingly, significant groundwater upwelling flow occurred even without evaporation effects on the surface where the groundwater system was mainly driven by the lateral hydraulic gradient (Figure 3f). The results provide evidence that local heterogeneity also contributed to the upwelling of the flow and solute from deep sediments toward the surface. By contrast, the upward movement of the solute was limited within areas of low permeability (Figures 3g and 3h). As a result, the solute concentration remained low near the surface where the sediment exhibited low permeability. Within those areas, the solute concentration was primarily increased by the spreading and dispersion of the high-concentration solute from the surrounding high-permeability zones, rather than by upward intrusion. The vertical concentration profiles further demonstrate the temporal evolution of the solute concentration along the depth for homogeneous and heterogeneous cases (Figures 3i and 3j). It is evident that multiple phases were involved in the upward intrusion of the solute from deep sediments by evaporation. Evaporation-induced groundwater upwelling transported the solute from deep sediments toward the surface. Once the solute reached the surface, evaporation accumulated it and increased its concentration at the surface. As the near-surface concentration exceeded that of the underlying layer, reversed concentration gradients caused the solute plume to disperse downwards. After 17 days of alternating evaporation, the solute concentration near the surface increased to over twice the initial concentration in deep sediments. In the homogeneous and heterogeneous cases, the surface concentration was 1.24 mg/L and 1.43 mg/L, respectively. The higher concentration in the heterogeneous case was due to preferential flow pathways, which allowed the solute to travel a shorter time to reach the surface and therefore increased its exposure time to evaporation at the surface. This enhanced the solute's accumulation near the surface. Figure 3k shows that the solute plume took 173 and 104 hr to migrate from deep sediment to the surface in the homogeneous and heterogeneous cases, respectively. It is evident that the shorter travel time in the heterogeneous case allowed the solute to undergo three additional evaporation cycles at the surface compared to the homogeneous case.

The combined effects of alternating evaporation and local heterogeneity lead to the emergence of complex mixing mechanisms in shallow wetland sediments. In the absence of evaporation, a contour plot of the Θ parameter shows that local heterogeneity created spatially varied strain- and vorticity-dominated flow regions. These regions coexisted at small spatial scales, mostly along the lateral preferential flow paths within high-permeability zones (Figure 4a). The solute mixing within sediment pores was intensified in the strain-dominated flow regions and limited in the vorticity-dominated flow regions. Evaporation intensified subsurface mixing and caused changes in its spatial patterns within sediments (Figure 4b). Due to evaporation, the strain- and vorticity-dominated flow regions experienced quantitative enhancement near the sediment surface and expanded further downwards along the vertical preferential flow pathways. This indicates that the solute underwent more intense stretching and deformation as it moved toward the surface. Additionally, evaporation increased the spatial extent of both the strain- and vorticity-dominated regions in the subsurface by 47% and 50%, respectively, compared to their extents in the absence of evaporation effects (Figure 4c). The dilution index further illustrates the impact of evaporation on subsurface mixing patterns (Figures 4d and 4e). In the absence of evaporation, high dilution index values were typically concentrated along lateral preferential groundwater flow pathways. However, evaporation on the sediment surface notably affected the spatial distribution of the dilution index. Due to evaporation, the values of the dilution index were significantly elevated near the sediment surface and expanded downward along the upward preferential flow pathways. Figure 4f demonstrates that the area of zones with the dilution index greater than 0.01 expanded by over threefold when evaporation occurred on the surface. Additionally, the average of the dilution index across the simulated domain nearly tripled, increasing from 6.2×10^{-3} to 1.7×10^{-2} due to evaporation. This indicates that evaporation-induced groundwater upwelling through the heterogeneous sediments created distinct mixing hotspots that spatially differed from those generated by lateral preferential flows driven by the large-scale hydraulic gradients. Overall, these results suggest that evaporation generally enhanced the mixing of groundwater and solute in the subsurface.

4. Discussion

Our study highlights the important role of evaporation in the upwelling of groundwater flow and solutes from deep sediments toward the surface in shallow wetlands. Previous studies have identified the accumulation of nutrients in deep wetland sediments (Brodersen et al., 2019; Davidsson et al., 1997; Senga et al., 2011; Visscher et al., 1991). Senga et al. (2011) found an accumulation of nitrate (NO_3^-) and dissolved organic carbon in deep

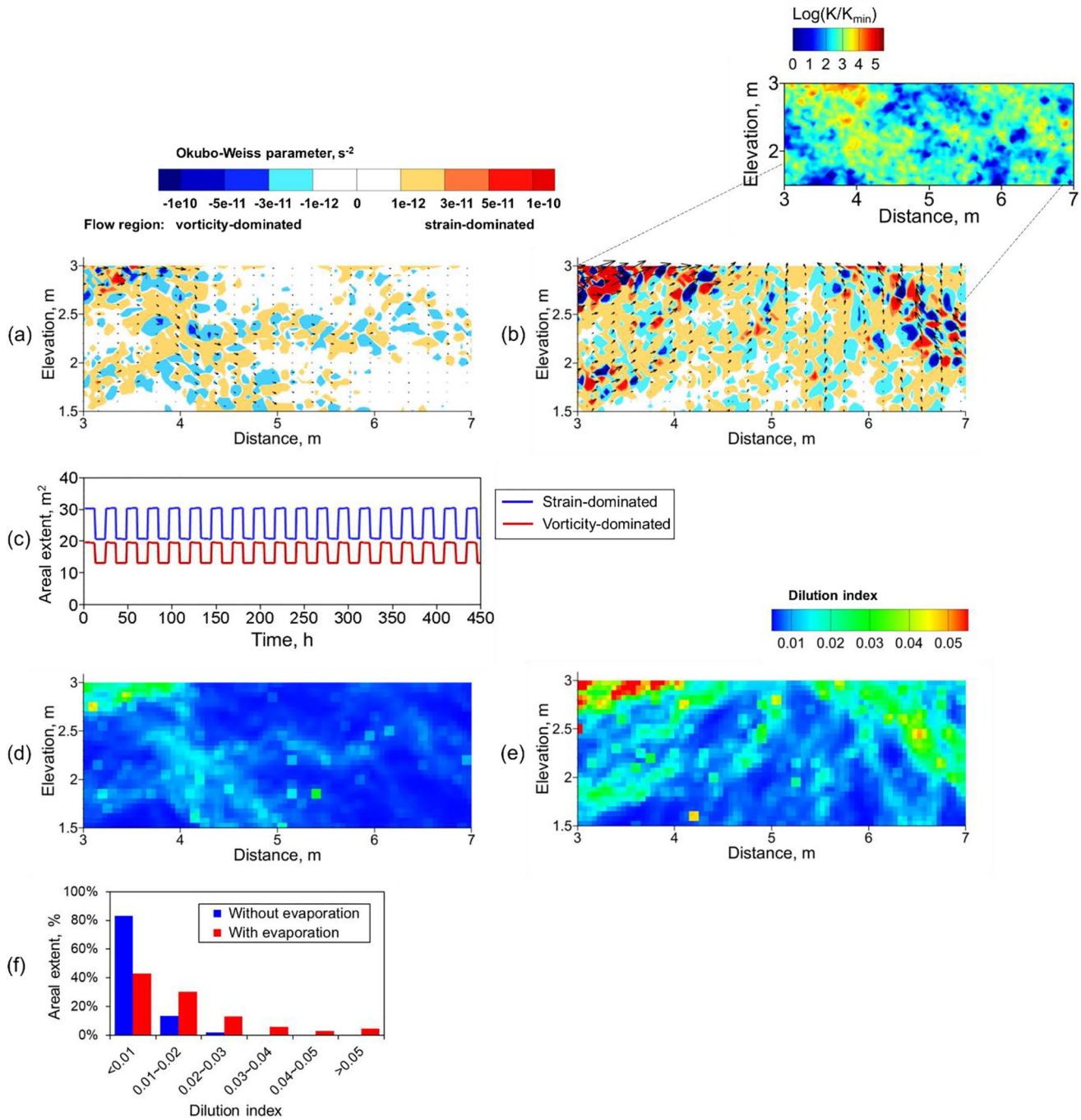

Figure 4. Distributions of (a, b) Okubo-Weiss parameter values, (c) their areal extent, (d–e) dilution index, and (f) areal extent of the zones with different dilution index (% of the total area) for the heterogeneous case without and with evaporation, respectively.

sediments of wetlands in northeastern Japan, attributed to an increase in nutrient loading from changes in land use. Brodersen et al. (2019) measured a high total sulfide (S^{2-}_{total}) concentration at deep locations of salt marshes. In this paper, we delineate, for the first time, evaporation could induce groundwater upwelling that drives the solute to transport from deep sediments to the surface; once the solute plume approaches the surface, evaporation will further enhance the accumulation of the solute near the surface and increase the solute concentration even higher than that in deep sediments. Note that we neglect the evaporation process during the night as its rate is typically much lower than during the day. However, in scenarios where overnight evaporation cannot be considered

negligible and is substantial, the evaporation-inducing upwelling flow and the consequent accumulation of solute near the surface will become even more prominent. Such transport mechanisms would strongly affect biogeochemical conditions in near-surface sediments of shallow wetlands. For instance, the accumulation of nutrients would cause acidification and eutrophication in surface sediments (Senga et al., 2011). The resulting change in nutrient concentrations and pore-water pH might cause the alternation of near-surface microbial communities as well as their activities associated with organic matter decomposition and nutrient remobilization and cycling (D'Angelo & Reddy, 1994; McLatchey & Reddy, 1998). Local heterogeneity creates preferential flow pathways through high-permeability regions which greatly shortens the travel time of the solute from deep sediments to the surface, which facilitates the accumulation of the solute near the sediment surface. Heterogeneity also causes spatial variability of solute upwelling from deep sediments and associated accumulation in surface sediments. This indicates the significant impacts of local heterogeneity on large-scale patterns of nutrient distributions in wetland sediments.

Our results reveal the flow topology and associated complex mixing dynamics in heterogeneous shallow wetland sediments induced by evaporation. We use the Okubo-Weiss parameter to show that local heterogeneity creates both strain-dominated and vorticity-dominated flow regions in wetland sediments. Their coexistence provides a critical control on the centimeter-scale mixing of water and solute within sediment pores. Solutes undergo stretching and deformation as they transport through strain-dominated flow regions, which leads to relatively high mixing within sediment pores (de Barros et al., 2012; Dentz et al., 2018; Weeks & Sposito, 1998). By contrast, the solutes experience rotation with less mixing as they travel through hotspots of vorticity-dominated flow regions. Such local-scale mixing patterns show a dynamic response to evaporation. The subsurface mapping of the dilution index suggests that evaporation-induced groundwater upwelling through the heterogeneous porous medium creates distinct mixing hotspots that spatially differed from those generated by lateral preferential flows driven by the large-scale hydraulic gradients. Such alternating spatial patterns of the dilution distribution enhance the mixing of groundwater and solute in the subsurface. Biogeochemical hotspots in wetland environments have been observed in numerous field studies (Larkin et al., 2016; McClain et al., 2003; Opdekamp et al., 2012; Palta et al., 2014). Our results indicate that the combined effects of evaporation and heterogeneity create dynamic mixing hotspots, which likely intensify complex mixing-dependent geochemical reactivity in shallow wetland sediments. It might provide plausible interpretations for these field observations, which have strong implications for biogeochemical processing in wetland environments. In this paper, our investigation focused on a groundwater system primarily influenced by lateral terrestrial groundwater discharge and evaporation, which is expected to exhibit mainly 2D behavior. While geologic heterogeneity may introduce some 3D perturbation to groundwater flow, the impacts of such effects are anticipated to be minimal when compared to the dominant hydraulic gradients. However, in certain highly heterogeneous aquifers, groundwater flow can exhibit significant 3D behavior (Geng & Michael, 2020; Kreyns et al., 2020; Perriquet et al., 2014), which needs to be considered in future studies. Nevertheless, it is important to note that significant upwelling of contaminants from deep sediments to the surface has not been fully recognized. Our simulation unveils a vital mechanism by which deep contaminants upwell in wetlands, underscoring the importance of considering this factor in future field monitoring efforts.

5. Conclusion

Groundwater flow simulations were conducted to show the combined effects of evaporation and local heterogeneity on the emergence of complex mixing mechanisms in shallow wetland sediments. Evaporation causes the upwelling of groundwater and solutes from deep sediments to the surface. As the solute plume approaches the surface, evaporation will further enhance the accumulation of the solute near the surface and increase the solute concentration even higher than that in deep sediments. The mapping of the flow topology, including the Okubo-Weiss parameter and dilution index, reveals that evaporation-induced groundwater upwelling through the heterogeneous porous medium likely creates distinct mixing hotspots that spatially differed from those generated by lateral preferential flows driven by the large-scale hydraulic gradients. Our findings highlight the necessity of taking into account evaporation and local heterogeneity in terms of evaluating wetland ecosystems.

Data Availability Statement

Data supporting this study are available in CUAHSI HydroShare (http://www.hydroshare.org/resource/135b355a2aec44c49308b463eee5decc).

Acknowledgments
This work was funded by the US NSF (Division of Earth Sciences [EAR] #2130595). However, it does not necessarily reflect the views of the funding agency, and no official endorsement should be inferred. This is SOEST contribution #11707.

References

Armstrong, W., Wright, E., Lythe, S., & Gaynard, T. (1985). Plant zonation and the effects of the spring-neap tidal cycle on soil aeration in a Humber salt marsh. *Journal of Ecology*, *73*(1), 323–339. https://doi.org/10.2307/2259786

Balke, T., Stock, M., Jensen, K., Bouma, T. J., & Kleyer, M. (2016). A global analysis of the seaward salt marsh extent: The importance of tidal range. *Water Resources Research*, *52*(5), 3775–3786. https://doi.org/10.1002/2015wr018318

Bhowmik, S. (2022). Ecological and economic importance of wetlands and their vulnerability: A review. *Research Anthology on Ecosystem Conservation and Preserving Biodiversity*, 11–27. https://doi.org/10.4018/978-1-6684-5678-1.ch002

Boufadel, M. C., Lu, S., Molz, F. J., & Lavallee, D. (2000). Multifractal scaling of the intrinsic permeability. *Water Resources Research*, *36*(11), 3211–3222. https://doi.org/10.1029/2000wr900208

Boufadel, M. C., Suidan, M. T., & Venosa, A. D. (1999). A numerical model for density-and-viscosity-dependent flows in two-dimensional variably saturated porous media. *Journal of Contaminant Hydrology*, *37*(1–2), 1–20. https://doi.org/10.1016/s0169-7722(98)00164-8

Brodersen, K. E., Trevathan-Tackett, S. M., Nielsen, D. A., Connolly, R. M., Lovelock, C. E., Atwood, T. B., & Macreadie, P. I. (2019). Oxygen consumption and sulfate reduction in vegetated coastal habitats: Effects of physical disturbance. *Frontiers in Marine Science*, *6*, 14. https://doi.org/10.3389/fmars.2019.00014

Castle, J. W., Molz, F. J., Lu, S., & Dinwiddie, C. L. (2004). Sedimentology and fractal-based analysis of permeability data, John Henry member, Straight Cliffs formation (upper Cretaceous), Utah, USA. *Journal of Sedimentary Research*, *74*(2), 270–284. https://doi.org/10.1306/082803740270

D'Angelo, E., & Reddy, K. (1994). Diagenesis of organic matter in a wetland receiving hypereutrophic lake water: II. Role of inorganic electron acceptors in nutrient release. *Journal of Environmental Quality*, *23*(5), 937–943. https://doi.org/10.2134/jeq1994.00472425002300050014x

Davidsson, T. E., Stepanauskas, R., & Leonardson, L. (1997). Vertical patterns of nitrogen transformations during infiltration in two wetland soils. *Applied and Environmental Microbiology*, *63*(9), 3648–3656. https://doi.org/10.1128/aem.63.9.3648-3656.1997

Davy, A. J., Brown, M. J., Mossman, H. L., & Grant, A. (2011). Colonization of a newly developing salt marsh: Disentangling independent effects of elevation and redox potential on halophytes. *Journal of Ecology*, *99*(6), 1350–1357. https://doi.org/10.1111/j.1365-2745.2011.01870.x

de la Fuente, A., & Meruane, C. (2017). Spectral model for long-term computation of thermodynamics and potential evaporation in shallow wetlands. *Water Resources Research*, *53*(9), 7696–7715. https://doi.org/10.1002/2017wr020515

de Barros, F. P., Dentz, M., Koch, J., & Nowak, W. (2012). Flow topology and scalar mixing in spatially heterogeneous flow fields. *Geophysical Research Letters*, *39*(8), L08404. https://doi.org/10.1029/2012gl051302

Dentz, M., de Barros, F., Le Borgne, T., & Lester, D. (2018). Evolution of solute blobs in heterogeneous porous media. *Journal of Fluid Mechanics*, *853*, 621–646. https://doi.org/10.1017/jfm.2018.588

Doss, P. K. (1993). The nature of a dynamic water table in a system of non-tidal, freshwater coastal wetlands. *Journal of Hydrology*, *141*(1–4), 107–126. https://doi.org/10.1016/0022-1694(93)90046-c

Douglas, M. M., Bunn, S. E., & Davies, P. M. (2005). River and wetland food webs in Australia's wet–dry tropics: General principles and implications for management. *Marine and Freshwater Research*, *56*(3), 329–342. https://doi.org/10.1071/mf04084

Geng, X., & Boufadel, M. C. (2015). Numerical modeling of water flow and salt transport in bare saline soil subjected to evaporation. *Journal of Hydrology*, *524*, 427–438. https://doi.org/10.1016/j.jhydrol.2015.02.046

Geng, X., & Boufadel, M. C. (2017). The influence of evaporation and rainfall on supratidal groundwater dynamics and salinity structure in a sandy beach. *Water Resources Research*, *53*(7), 6218–6238. https://doi.org/10.1002/2016wr020344

Geng, X., Boufadel, M. C., & Jackson, N. L. (2016a). Evidence of salt accumulation in beach intertidal zone due to evaporation. *Scientific Reports*, *6*(1), srep31486. https://doi.org/10.1038/srep31486

Geng, X., Boufadel, M. C., Lee, K., & An, C. (2020). Characterization of pore water flow in 3D heterogeneous permeability fields. *Geophysical Research Letters*, *47*(3), e2019GL086879. https://doi.org/10.1029/2019gl086879

Geng, X., Boufadel, M. C., Ozgokmen, T., King, T., Lee, K., Lu, Y., & Zhao, L. (2016b). Oil droplets transport due to irregular waves: Development of large-scale spreading coefficients. *Marine Pollution Bulletin*, *104*(1–2), 279–289. https://doi.org/10.1016/j.marpolbul.2016.01.007

Geng, X., Boufadel, M. C., Rajaram, H., Cui, F., Lee, K., & An, C. (2020). Numerical study of solute transport in heterogeneous beach aquifers subjected to tides. *Water Resources Research*, *56*(3), e2019WR026430. https://doi.org/10.1029/2019wr026430

Geng, X., Boufadel, M. C., Xia, Y., Li, H., Zhao, L., Jackson, N. L., & Miller, R. S. (2014). Numerical study of wave effects on groundwater flow and solute transport in a laboratory beach. *Journal of Contaminant Hydrology*, *165*, 37–52. https://doi.org/10.1016/j.jconhyd.2014.07.001

Geng, X., Heiss, J. W., Michael, H. A., Boufadel, M. C., & Lee, K. (2020). Groundwater flow and moisture dynamics in the swash zone: Effects of heterogeneous hydraulic conductivity and capillarity. *Water Resources Research*, *56*(11), e2020WR028401. https://doi.org/10.1029/2020WR028401

Geng, X., & Michael, H. A. (2020). Preferential flow enhances pumping-induced saltwater intrusion in volcanic aquifers. *Water Resources Research*, *56*(5), e2019WR026390. https://doi.org/10.1029/2019wr026390

Geng, X., Michael, H. A., Boufadel, M. C., Molz, F. J., Gerges, F., & Lee, K. (2020). Heterogeneity affects intertidal flow topology in coastal beach aquifers. *Geophysical Research Letters*, *47*(17), e2020GL089612. https://doi.org/10.1029/2020gl089612

Geng, X., Pan, Z., Boufadel, M. C., Ozgokmen, T., Lee, K., & Zhao, L. (2016). Simulation of oil bioremediation in a tidally influenced beach: Spatiotemporal evolution of nutrient and dissolved oxygen. *Journal of Geophysical Research: Oceans*, *121*(4), 2385–2404. https://doi.org/10.1002/2015jc011221

Ghiat, I., Mackey, H. R., & Al-Ansari, T. (2021). A review of evapotranspiration measurement models, techniques and methods for open and closed agricultural field applications. *Water*, *13*(18), 2523. https://doi.org/10.3390/w13182523

Guimond, J., & Tamborski, J. (2021). Salt marsh hydrogeology: A review. *Water*, *13*(4), 543. https://doi.org/10.3390/w13040543

Guimond, J. A., Yu, X., Seyfferth, A. L., & Michael, H. A. (2020). Using hydrological-biogeochemical linkages to elucidate carbon dynamics in coastal marshes subject to relative sea level rise. *Water Resources Research*, *56*(2), e2019WR026302. https://doi.org/10.1029/2019wr026302

Harvey, J. W., Chambers, R. M., & Hoelscher, J. R. (1995). Preferential flow and segregation of porewater solutes in wetland sediment. *Estuaries*, *18*(4), 568–578. https://doi.org/10.2307/1352377

Harvey, J. W., & Nuttle, W. K. (1995). Fluxes of water and solute in a coastal wetland sediment. 2. Effect of macropores on solute exchange with surface water. *Journal of Hydrology*, *164*(1–4), 109–125. https://doi.org/10.1016/0022-1694(94)02562-p

Isern-Fontanet, J., Font, J., García-Ladona, E., Emelianov, M., Millot, C., & Taupier-Letage, I. (2004). Spatial structure of anticyclonic eddies in the Algerian basin (Mediterranean Sea) analyzed using the Okubo–Weiss parameter. *Deep Sea Research Part II: Topical Studies in Oceanography*, *51*(25–26), 3009–3028. https://doi.org/10.1016/j.dsr2.2004.09.013

Kitanidis, P. K. (1994). The concept of the dilution index. *Water Resources Research*, *30*(7), 2011–2026. https://doi.org/10.1029/94wr00762

Kreyns, P., Geng, X., & Michael, H. A. (2020). The influence of connected heterogeneity on groundwater flow and salinity distributions in coastal volcanic aquifers. *Journal of Hydrology*, *124863*, 124863. https://doi.org/10.1016/j.jhydrol.2020.124863
Larkin, D. J., Bruland, G. L., & Zedler, J. B. (2016). Heterogeneity theory and ecological restoration. *Foundations of Restoration Ecology*, 271–300. https://doi.org/10.5822/978-1-61091-698-1_10
Li, H., Boufadel, M. C., & Weaver, J. W. (2008). Tide-induced seawater–groundwater circulation in shallow beach aquifers. *Journal of Hydrology*, *352*(1–2), 211–224. https://doi.org/10.1016/j.jhydrol.2008.01.013
Li, H., Li, L., & Lockington, D. (2005). Aeration for plant root respiration in a tidal marsh. *Water Resources Research*, *41*(6). https://doi.org/10.1029/2004wr003759
Liu, S., Mao, D., & Lu, L. (2006). Measurement and estimation of the aerodynamic resistance. *Hydrology and Earth System Sciences Discussions*, *3*, 681–705.
Liu, Y., Zhang, C., Liu, X., Li, C., Sheuermann, A., Xin, P., et al. (2022). Salt transport under tide and evaporation in a subtropical wetland: Field monitoring and numerical simulation. *Water Resources Research*, *58*(5), e2021WR031530. https://doi.org/10.1029/2021wr031530
Mahfouf, J., & Noilhan, J. (1991). Comparative study of various formulations of evaporations from bare soil using in situ data. *Journal of Applied Meteorology*, *30*(9), 1354–1365. https://doi.org/10.1175/1520-0450(1991)030<1354:csovfo>2.0.co;2
McClain, M. E., Boyer, E. W., Dent, C. L., Gergel, S. E., Grimm, N. B., Groffman, P. M., et al. (2003). Biogeochemical hot spots and hot moments at the interface of terrestrial and aquatic ecosystems. *Ecosystems*, *6*(4), 301–312. https://doi.org/10.1007/s10021-003-0161-9
McLatchey, G. P., & Reddy, K. (1998). *Regulation of organic matter decomposition and nutrient release in a wetland soil (No. 0047–2425)*. Wiley Online Library.
Moffett, K. B., Gorelick, S. M., McLaren, R. G., & Sudicky, E. A. (2012). Salt marsh ecohydrological zonation due to heterogeneous vegetation–groundwater–surface water interactions. *Water Resources Research*, *48*(2). https://doi.org/10.1029/2011wr010874
Opdekamp, W., Teuchies, J., Vrebos, D., Chormański, J., Schoelynck, J., Van Diggelen, R., et al. (2012). Tussocks: Biogenic silica hot-spots in a riparian wetland. *Wetlands*, *32*(6), 1115–1124. https://doi.org/10.1007/s13157-012-0341-5
Palta, M. M., Ehrenfeld, J. G., & Groffman, P. M. (2014). Hotspots" and "hot moments" of denitrification in urban brownfield wetlands. *Ecosystems*, *17*(7), 1121–1137. https://doi.org/10.1007/s10021-014-9778-0
Pecknold, S., Lovejoy, S., Schertzer, D., Hooge, C., & Malouin, J. (1993). *The simulation of universal multifractals* (pp. 228–267). Presented at the Cellular Automata.
Peitgen, H.-O., & Saupe, D. (1988). *The science of fractal images*. Springer-Verlag New York, Inc.
Perriquet, M., Leonardi, V., Henry, T., & Jourde, H. (2014). Saltwater wedge variation in a non-anthropogenic coastal karst aquifer influenced by a strong tidal range (Burren, Ireland). *Journal of Hydrology*, *519*, 2350–2365. https://doi.org/10.1016/j.jhydrol.2014.10.006
Richardson, C. J. (1994). Ecological functions and human values in wetlands: A framework for assessing forestry impacts. *Wetlands*, *14*, 1–9. https://doi.org/10.1007/bf03160616
Sadat-Noori, M., & Glamore, W. (2019). Porewater exchange drives trace metal, dissolved organic carbon and total dissolved nitrogen export from a temperate mangrove wetland. *Journal of Environmental Management*, *248*, 109264. https://doi.org/10.1016/j.jenvman.2019.109264
Sawyer, A. (2015). Enhanced removal of groundwater-borne nitrate in heterogeneous aquatic sediments. *Geophysical Research Letters*, *42*(2), 403–410. https://doi.org/10.1002/2014gl062234
Schertzer, D., & Lovejoy, S. (1987). Physical modeling and analysis of rain and clouds by anisotropic scaling multiplicative processes. *Journal of Geophysical Research*, *92*(D8), 9693–9714. https://doi.org/10.1029/jd092id08p09693
Schertzer, D., & Lovejoy, S. (2011). Multifractals, generalized scale invariance and complexity in geophysics. *International Journal of Bifurcation and Chaos*, *21*(12), 3417–3456. https://doi.org/10.1142/s0218127411030647
Senga, Y., Hiroki, M., Nakamura, Y., Watarai, Y., Watanabe, Y., & Nohara, S. (2011). Vertical profiles of DIN, DOC, and microbial activities in the wetland soil of Kushiro Mire, northeastern Japan. *Limnology*, *12*(1), 17–23. https://doi.org/10.1007/s10201-010-0316-2
Silvestri, S., Defina, A., & Marani, M. (2005). Tidal regime, salinity and salt marsh plant zonation. *Estuarine, Coastal and Shelf Science*, *62*(1–2), 119–130. https://doi.org/10.1016/j.ecss.2004.08.010
Sposito, G. (2001). Topological groundwater hydrodynamics. *Advances in Water Resources*, *24*(7), 793–801. https://doi.org/10.1016/s0309-1708(00)00077-4
Tessier, Y., Lovejoy, S., & Schertzer, D. (1993). Universal multifractals: Theory and observations for rain and clouds. *Journal of Applied Meteorology*, *32*(2), 223–250. https://doi.org/10.1175/1520-0450(1993)032<0223:umtaof>2.0.co;2
Thibodeau, P. M., Gardner, L. R., & Reeves, H. W. (1998). The role of groundwater flow in controlling the spatial distribution of soil salinity and rooted macrophytes in a southeastern salt marsh, USA. *Mangroves and Salt Marshes*, *2*, 1–13. https://doi.org/10.1023/a:1009910712539
Visscher, P. T., Beukema, J., & van Gemerden, H. (1991). In situ characterization of sediments: Measurements of oxygen and sulfide profiles with a novel combined needle electrode. *Limnology & Oceanography*, *36*(7), 1476–1480. https://doi.org/10.4319/lo.1991.36.7.1476
Wang, F., Xiao, K., Santos, I. R., Lu, Z., Tamborski, J., Wang, Y., et al. (2022). Porewater exchange drives nutrient cycling and export in a mangrove-salt marsh ecotone. *Journal of Hydrology*, *606*, 127401. https://doi.org/10.1016/j.jhydrol.2021.127401
Wang, Z. A., & Cai, W. (2004). Carbon dioxide degassing and inorganic carbon export from a marsh-dominated estuary (the Duplin river): A marsh CO2 pump. *Limnology & Oceanography*, *49*(2), 341–354. https://doi.org/10.4319/lo.2004.49.2.0341
Weeks, S. W., & Sposito, G. (1998). Mixing and stretching efficiency in steady and unsteady groundwater flows. *Water Resources Research*, *34*(12), 3315–3322. https://doi.org/10.1029/98wr02535
Wilson, A. M., Evans, T., Moore, W., Schutte, C. A., Joye, S. B., Hughes, A. H., & Anderson, J. L. (2015). Groundwater controls ecological zonation of salt marsh macrophytes. *Ecology*, *96*(3), 840–849. https://doi.org/10.1890/13-2183.1
Wilson, A. M., & Gardner, L. R. (2006). Tidally driven groundwater flow and solute exchange in a marsh: Numerical simulations. *Water Resources Research*, *42*(1). https://doi.org/10.1029/2005wr004302
Xiao, K., Li, H., Xia, Y., Yang, J., Wilson, A. M., Michael, H. A., et al. (2019). Effects of tidally varying salinity on groundwater flow and solute transport: Insights from modelling an idealized creek marsh aquifer. *Water Resources Research*, *55*(11), 9656–9672. https://doi.org/10.1029/2018wr024671
Xin, P., Wilson, A., Shen, C., Ge, Z., Moffett, K. B., Santos, I. R., et al. (2022). Surface water and groundwater interactions in salt marshes and their impact on plant ecology and coastal biogeochemistry. *Reviews of Geophysics*, *60*(1), e2021RG000740. https://doi.org/10.1029/2021rg000740
Xin, P., Zhou, T., Lu, C., Shen, C., Zhang, C., D'Alpaos, A., & Li, L. (2017). Combined effects of tides, evaporation and rainfall on the soil conditions in an intertidal creek-marsh system. *Advances in Water Resources*, *103*, 1–15. https://doi.org/10.1016/j.advwatres.2017.02.014
Xu, X., Xin, P., Zhou, T., & Xiao, K. (2021). Effect of macropores on pore-water flow and soil conditions in salt marshes subject to evaporation and tides. Estuarine. *Coastal and Shelf Science*, *261*, 107558. https://doi.org/10.1016/j.ecss.2021.107558
Zedler, J. B., Callaway, J. C., Desmond, J. S., Vivian-Smith, G., Williams, G. D., Sullivan, G., et al. (1999). Californian salt-marsh vegetation: An improved model of spatial pattern. *Ecosystems*, *2*(1), 19–35. https://doi.org/10.1007/s100219900055

Zhang, C., Li, L., & Lockington, D. (2014). Numerical study of evaporation-induced salt accumulation and precipitation in bare saline soils: Mechanism and feedback. *Water Resources Research*, *50*(10), 8084–8106. https://doi.org/10.1002/2013wr015127

Zhao, S., Zhou, N., & Shen, X. (2016). Driving mechanisms of nitrogen transport and transformation in lacustrine wetlands. *Science China Earth Sciences*, *59*(3), 464–476. https://doi.org/10.1007/s11430-015-5230-3

Zheng, C., & Bennett, G. D. (2002). *Applied contaminant transport modelling*. John Wiley and Sons.

Erratum

In the originally published version of this article, the contribution number from the author's institution (SOEST #11707) was omitted from the Acknowledgments. The error has been corrected, and this may be considered the authoritative version of record.